JOURNAL OF MATERIALS SCIENCE **33** (1998) 5311–5325

On the failure of unidirectional carbon-epoxy composites Part I: The effect of fibre sizing upon filament fracture and damage evolution

C. MARSTON*
School of Engineering Systems Design, South Bank University, London, SE1 OAA, UK

C. GALIOTIS†
Institute of Chemical Engineering and High Temperature Processes, Foundation for Research & Technology – Hellas, Stadiou Street, Platani, P.O. Box 1414, GR-265 00, Patras, Greece and Materials Department, Queen Mary & Westfield College, Mile End Road, London E1 4NS, UK

It has been demonstrated that – in certain cases – the sizing of carbon fibres can have a dramatic effect upon the mode of failure of unidirectional fibre-reinforced composites. The sizing appears to reduce the strength of composite tows by confining the failure process to a very small area that exhibits high stress concentration. In this paper, the effect of fibre sizing upon the two-dimensional fibre break density and break cluster populations is investigated as a function of applied strain prior to composite failure. It is shown that the size of the damage sites, their spatial distribution in the composite and the alignment between the individual breaks in the cluster are affected by the interface properties. Fractographic analysis has shown that groups of adjacent fibre fractures of greater than three were observed for the sized composite tows, whereas for the unsized samples a higher proportion of single and double breaks were seen to exist at a particular stress level. As a result, the overall filament damage was seen to be more widespread in the case of the unsized composite tows. Two possible mechanisms of fracture nucleation based on changes in fibre break density and in cluster populations are proposed: (a) failure due to growth of a critical cluster of fibre fractures and/or (b) linking up of several smaller cluster to form a critical cluster.

1. Introduction

Several probabilistic theories for the tensile strength of unidirectional composites have been proposed by Rosen [1], Rosen and Zweben [2], Smith [3], Harlow and Phoenix [4, 5], Bader [6] and Batdorf [7]. These models give satisfactory strength estimations when the composite failure is predominately controlled by the strength of the reinforcing fibres. However, the problem is far more complex as secondary fracture processes such as interface debonding and crack penetration into the matrix also affect composite failure. In many widely used classes of composites the fibre-matrix interface properties can govern the fracture processes and therefore the fibre-matrix interfacial shear strength can play a critical role in determining the tensile strength of the composite [8].

The final composite failure proceeds by progressive filament failure at a fraction of the ultimate composite failure load. In turn, the fibre failure is controlled by the statistical distribution of inherent fibre flaws. An appropriate description of this flaw population is given by the Weibull distribution of strengths for a brittle material [9]. Under increasing composite strain, the weakest fibre will eventually fracture when the fibre stress exceeds its local failure stress. The neighbouring surviving fibres adjacent to a break will be subject to a stress concentration, K_q, over a "positively affected length" (PAL) [10]. The stress concentration factor is the maximum stress of the fibre within PAL divided by the far field stress. Gao, Reifsnider and Carman [11] have postulated that in practice, values of stress concentration will vary for the same number of breaks for differing fibre/matrix systems. This stress overload increases the probability that a neighbouring fibre will fail. As the strain increases, the next weakest fibre fails and the density of the individual breaks will increase [1]. Some of these fracture sites start to develop into larger damage sites predominantly due to the presence of stress concentration in the adjacent fibres; these groups of fibre breaks will be referred here as 'clusters'. At a certain applied load, one of the larger cluster sites will evolve rapidly into an unstable microcrack

* Center for Composite Materials, University of Southern California, VHE#602, Los Angeles, California 90028-0241, USA.
† Author to whom all correspondence should be addressed. E-mail: c.galiotis@iceht.forth.gr.

leading to the final failure of the composite. Alternatively, a large number of smaller cluster sites can join to form the final failure path. The formation of filament cluster breaks and their subsequent growth, are influenced significantly by the local strength properties of the constituents and the load redistribution around filament breaks [12]. The stress redistribution from the broken fibre to the neighbouring – surviving – fibres is accomplished via shear in the matrix and, henceforth, depends upon how strongly the fibres adhere to the matrix. When the fibre/matrix bonding is weak, cracks can propagate along the interface of the fibres. When there is a strong fibre-matrix interaction shear or penny shape cracks may propagate into the matrix, at some angle θ ($90^\circ \geq \theta > 0^\circ$) to the fibre axis.

Fibre surface properties have been found to affect the adhesion of the fibres to the matrices, which in turn determine whether high shear loading can be supported [13]. The sizing on carbon fibre consists of a thin layer of usually epoxy resin, which protect the carbon fibre surface and enhances the interfacial properties. Drzal *et al.* [14] assumed that the presence of a coupling agent or sizing between the fibre and the matrix might promote the creation a brittle interphase around the fibre. This in turn could contribute to more efficient stress transfer in the reinforcing fibre.

2. Experimental

2.1. Material and specimen fabrication

Sized M40B-6K-40B and unsized M40B-6K-40B carbon fibres supplied by Soficar (France) were used in this study. The fibres were on average 6.6 μm in diameter. Single tows of the sized and unsized fibre were impregnated with a two-part LY-HY 5052 Ciba-Geigy epoxy resin. The LY-HY 5052 resin is an epoxy novolac and difunctional reactive diluent. The HY 5052 hardener is based on an cycloaliphatic amine with phenolic and organic acid accelerators present [15].

The simplest geometry of a unidirectional composite is that of fibre tow bundles impregnated with a resin. The resin (LY-5052) and hardener (HY-5052) were mixed at room temperature at a ratio of 4 : 1, degassed for 10 minutes under full vacuum and poured into a bath. Samples were cured for 24 hours at room temperature in accordance with the manufacturer's instructions [15]. Specimens were prepared by pulling the tows from the spool through a resin bath at room temperature, then through a 0.42 mm die to improve consolidation and control of the fibre volume fraction. The resulting material was a cylindrical rod of composite approximately 0.4 mm in diameter, with a fibre volume fraction of 55–60%. Impregnated tows of gauge length 130 mm were prepared for tensile testing by fitting glass fibre end-tabs [16]. The impregnated bundles were cured for 24 hours at room temperature in accordance with the manufacturer's instructions [15].

2.2. Mechanical loading of fibres and impregnated tows

The mechanical properties of all fibres were determined by single filament tests. Single fibres were peeled from the tow spool and then mounted by means of a cyanoacrylate glue on windows card types designated in ASTM D3379 [17]. The tensile strength and Young's modulus of single fibres from each batch was measured using an Instron 4507 machine. Approximately 55 measurements were made using fibres with a gauge length of 40 mm for each batch of sized and unsized filaments. An average fibre diameter of 6.6 μm was calculated by means of density measurements described elsewhere [16].

Experiments were conducted on sized M40B-6K-40B (MEBS) and unsized M40B-6K-40B (MUS) carbon/epoxy composite systems. Impregnated tows were prepared for tensile testing by fitting glass fibre end tabs. Approximately 40 impregnated bundle specimens of sized and unsized fibres at a gauge length of 130 mm were loaded on an Instron 4507 testing rig. The tensile strength variability, the stress redistribution profiles around filament failure, as well as, the fracture morphology [18–20] of the corresponding composite tows were investigated.

2.3. Fractographic investigation of impregnated tows

In order to investigate the build-up of fibre breaks during axial tension, sized and unsized tows of 130 mm gauge length were tested to pre-selected strain levels of 0.25%, 0.35% and 0.45%. Tow failure for this material system was known to occur at approximately 0.50% applied strain [19]. The damage was then analysed by sectioning longitudinally three 25 mm lengths of each specimen at all increments of applied strain. The specimens were subsequently polished on a rotary-grinding machine at a selection of paper grades and the area of damage was observed using a standard optical microscope. The number of individual breaks (or singlets), plus the fibre breaks adjacent to these singlets referred to as i-plets by Batdorf [7], were counted in a rectangular 'window' of 25 fibres in nominal specimen width by 20 mm in length. In addition, the relative offset between individual breaks in the cluster, as well as, their relative position in this window was also measured using the microscope stage to an accuracy of 1 μm. It is worth noting that with this method only fibre breaks situated at the surface or the near surface of the composite could be detected.

In this study a cluster is defined as several broken fibres or i-plets ($i > 1$) in a confined region. For example a single fibre break will be referred to as a singlet and a two fibre break as 2-plet or a cluster of 2 fibre breaks. Two adjacent filament failures are only part of the same cluster if their distance of separation falls within the PAL of the fibre i.e. twice the ineffective length 2δ, equal to 400 μm for the MEBS and 440 μm for the MUS composite systems. The schematic representation of the stress distribution in an assembly of a broken and an adjacent surviving fibre is given in Fig. 1.

2.4. Laser Raman microscopy

The technique of laser Raman spectroscopy (LRS) was employed for the measurement of the stress transfer

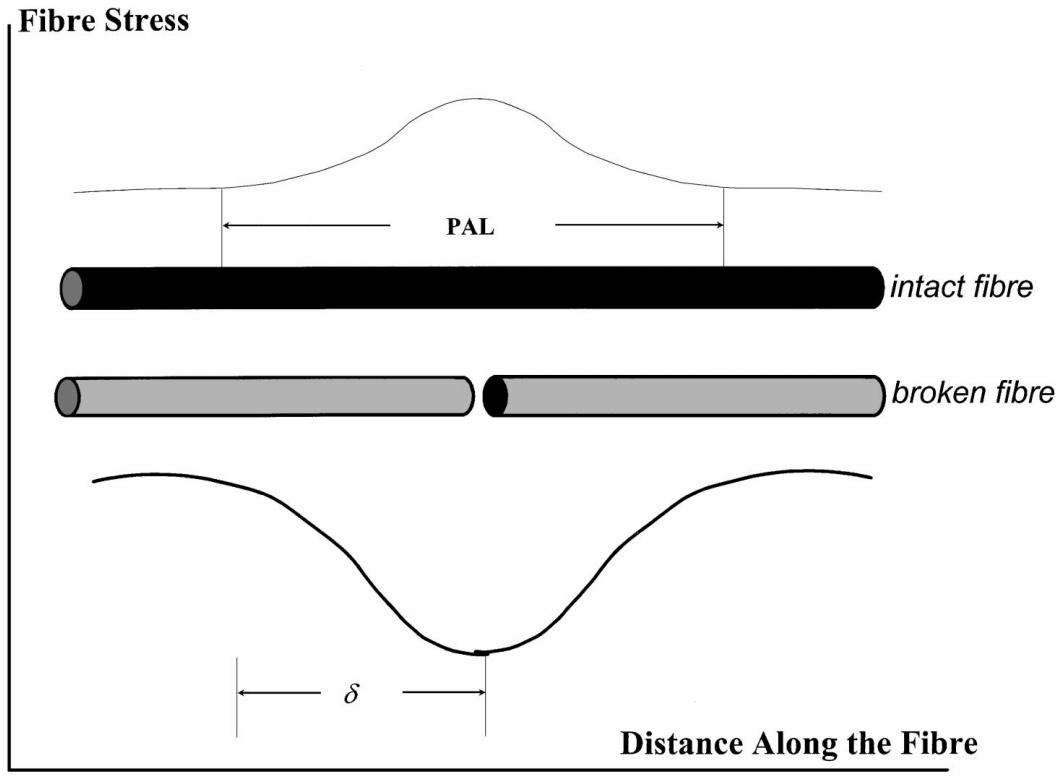

Figure 1 Schematic of stress distribution along a broken fibre and an adjacent surviving fibre. The ineffective length, δ, and the positively affected length, PAL, are shown.

profiles for the two fibre/matrix combinations and the effects of stress redistribution around fibre breaks [20].

Raman spectra were obtained using the 514.5 nm (green-line) of an Ar-ion laser as the excitation wavelength. The laser beam was directed through a series of mirrors to a modified Nikon microscope, which was used to focus the laser beam to a 2 μm spot on the fibre via a suitable objective lens. A laser power of 2 mW was used in the collection of the Raman spectra. The 180° back-scattered beam was collected by the same microscope objective and focused on the entrance slit of a SPEX 1877 triple monochromator spectrometer. To reduce the effective scattering volume to the region of the depth of focus in the fibre, the scattered beam was focused onto a 200 μm pinhole before it entered the spectrometer. Finally, the spectrometer dispersed light was directed to a Wright instruments CCD (Charged Couple Device) detector used as a photon detecting system and the Raman spectrum was recorded on a PC. All frequency peak values have been derived by applying Lorenzian fitting routines to the raw data obtained by the CCD detector.

The experimental data of the fibre stress versus distance along the specimen were fitted with b-spline polynomial curves [16]. The b-splines allow for discontinuity of derivatives at specific points. By use of a shear balance of forces model and differentiation of the fitted b-spline curves, the ISS profiles along individual fragments were derived [13].

Axial strain was applied to the composite tow by means of a specially designed microextensometer, which was mounted on the Raman microscope stage. The micrometer stage allowed translation of the specimen in all three axis down to an accuracy of 1 μm. The fibre stress within a Raman gauge length of 700 μm for an applied composite strain of 0.5% was mapped using the Raman microprobe. In Fig. 2a the failed MEBS fibre (number 4), as well as, the 3 fibres situated on either side of the fracture plane are shown. The fibre stress redistribution around a single MUS filament break at an applied composite strain of 0.6% is shown in Fig. 2b.

3. Results

3.1. Fibres in air

As reported elsewhere, the fibre strengths were found to follow a two-parameter Weibull distribution [9, 18]. Table I shows the strength data for single fibres, 40 mm in

TABLE I A summary of the Weibull modulus, w and the characteristic strength, σ_0 for failure stress of sized and unsized fibres recorded for single fibres and impregnated tows specimens

Sample	Surface treatment	Gauge length (mm)	No. of observations	Characteristic strength σ_0 (MPa)	Weibull parameter, w
Single fibres	Sized	40	138	2980	7.8
Single fibres	Unsized	40	152	2980	8.4
Tows	Sized	130	40	1790	15.0
Tows	Unsized	130	40	1919	18.2

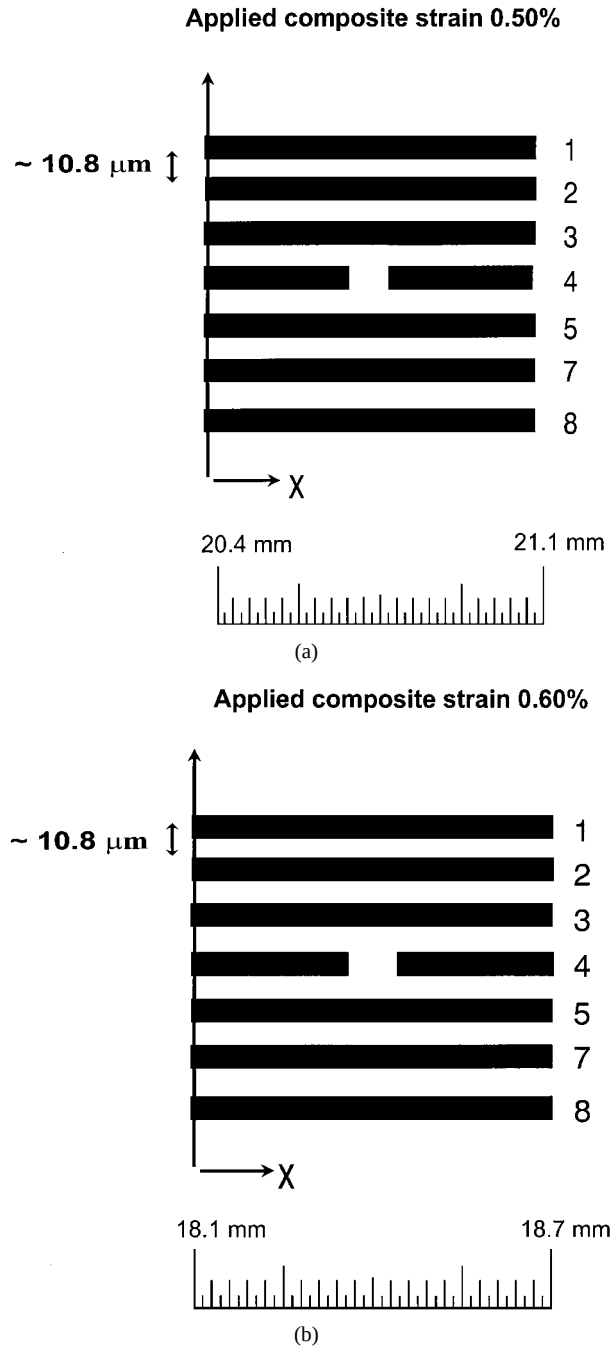

Figure 2 Schematic illustration of regions of stress mapping: (a) MEBS tow composite system and (b) MUS tow composite system.

gauge length, as well as, for sized and unsized composite tows 130 mm in gauge length. A Weibull Modulus of 13.5 and 11.5 was obtained for the single MEBS and MUS fibres, respectively, and the fibre sizing was not seen to affect significantly the individual filament strength (Table I).

3.2. Mechanical performance of impregnated tows

The values of measured Weibull Modulus of 15.0 and 18.2 for the MEBS and MUS impregnated bundles, respectively, showed that there was less variability in the strength of tows than for the fibres in air. It is worth noting also that the MEBS tows exhibited a wider scatter ($w = 15$) than the MUS tows ($w = 18.2$), which possibly indicates a different mechanism in the formation of a decisive flaw causing failure. The characteristic strength for failure of the sized MEBS system was 1790 MPa, thus lower by 7% of the corresponding value of the unsized MUS composite.

3.3. Stress distribution in the composite tows

Figs 3 and 4 show the stress distribution in fibres adjacent to a single filament break in the sized and unsized composite systems. In both cases (MEBS and MUS systems) the fibre stress drops to zero at the tip of the fibre break and then builds up from either side to reach a maximum value. The 'ineffective' lengths, δ, were approximately 200 and 220 μm for the MEBS and MUS systems, respectively (Figs 3 and 4). The positively affected length (PAL) was estimated to 2δ in both cases.

In Fig. 5 the stress concentration factors for the MEBS and MUS composite systems versus the interfibre distance is given. In the case of the single MEBS filament break a K_1 ($q = 1$) of 1.18 is observed for a nearest neighbour fibre (fibres 3 and 5) at an interfibre (centre-to-centre) distance of 10.8 μm. As the distance from the fibre break increases to 21.7 μm (fibre 2 and 6) the value of K_1 decreases to 1.14. At a distance of 32.6 μm a K_1 of approximately unity is observed in fibres 1 and 7. In the case of the MUS single filament break a stress concentration factor, K_1, of 1.14, 1.04, 1 is recorded for approximately the same (centre-to-centre) filament distances to those of the MEBS tow. The stress concentration values measured by LRS are comparable to those presented by Hedegepth [21] and Sastry and Phoenix [22] of 1.33 and 1.24, respectively. Fig. 6 shows the stress concentration factor, in the MEBS and MUS for $q = 2$ (double filament break) as a function of interfibre distance. In the MEBS tows a K_2 of approximately 1.33 was observed for a nearest neighbour fibre at a (centre-to-centre) interfibre distance of 10.9 μm from the two filament breaks. In the case of an unsized tow a stress overload of 1.18 was observed in the adjacent fibre to the double break at approximately the same interfibre distance.

The fibre stress profiles are converted into interfacial shear stress (ISS) distributions by employing a simple analytical expression between the ISS, and the gradient of the stress transfer profiles [23]. Fig. 7 shows the fibre interfacial shear stress for $q = 1$ for the MEBS and MUS systems shown in Figs 3 and 4. As can be seen, the ISS built up from zero at the tip of the fibre break to a maximum value of about 30 and 21 MPa for the MEBS and MUS fibres, respectively, and then decayed to zero at the middle of the fragment.

3.4. Optical fractography

Fig. 8 shows photomicrographs of the failure zone in a sized and unsized hybrid composite [19]. These are samples of composite tows surrounded by a glass fibre resin system. The glass fibre resin system has a higher failure strain than the impregnated tow, so that when the sample is loaded in tension, the tows fail first and remain supported by the surrounding material. The crack in the

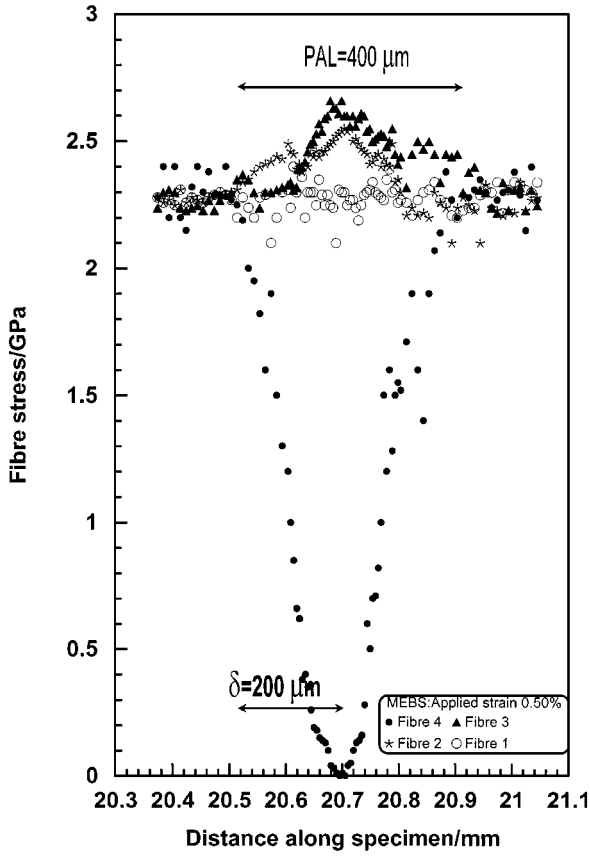

(a)

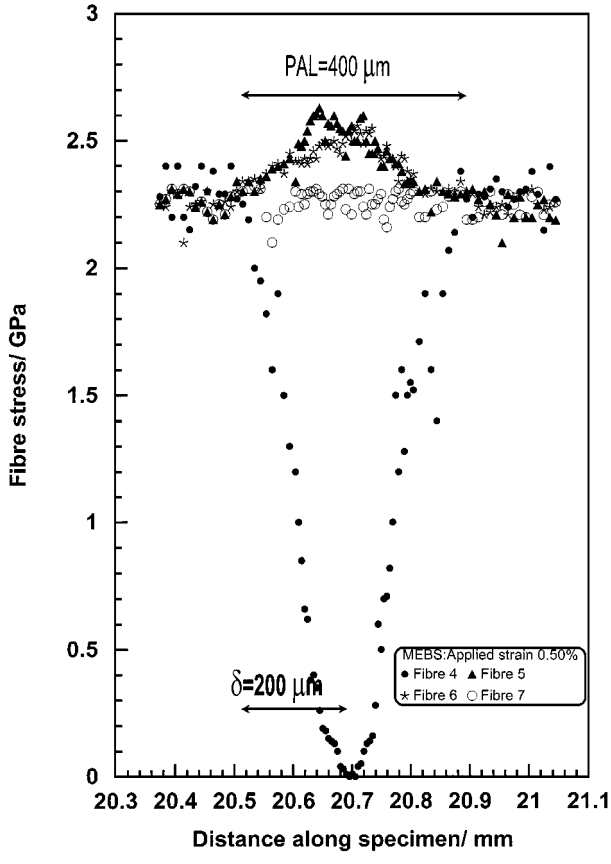

(b)

Figure 3 Fibre stress distribution in (a) fibres 4, 3, 2, and 1 for the MEBS tows of 'window' of Fig. 2a at 0.50% applied strain and (b) fibres 4, 5, 6, and 7 for the MEBS tows of 'window' of Fig. 2a at 0.50% applied strain.

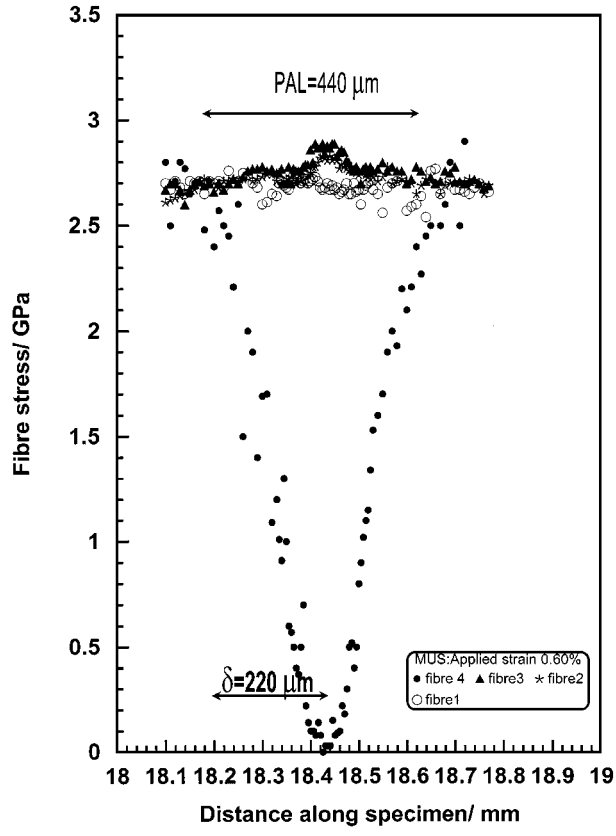

(a)

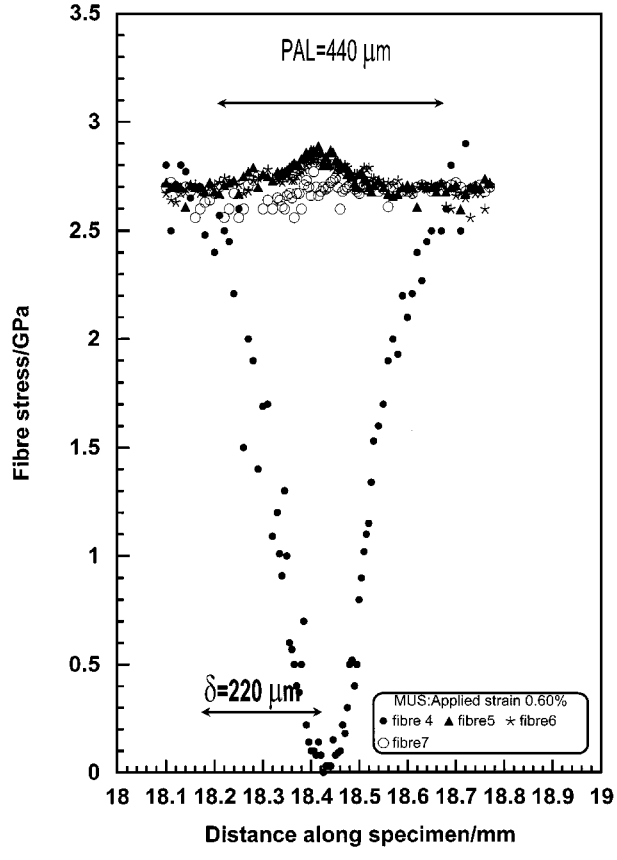

(b)

Figure 4 Fibre stress distribution in (a) fibres 4, 3, 2, and 1 for the MUS tows of 'window' of Fig. 2b at 0.60% applied strain and (b) fibres 4, 5, 6, and 7 for the MUS tows of 'window' of Fig. 2b at 0.60% applied strain.

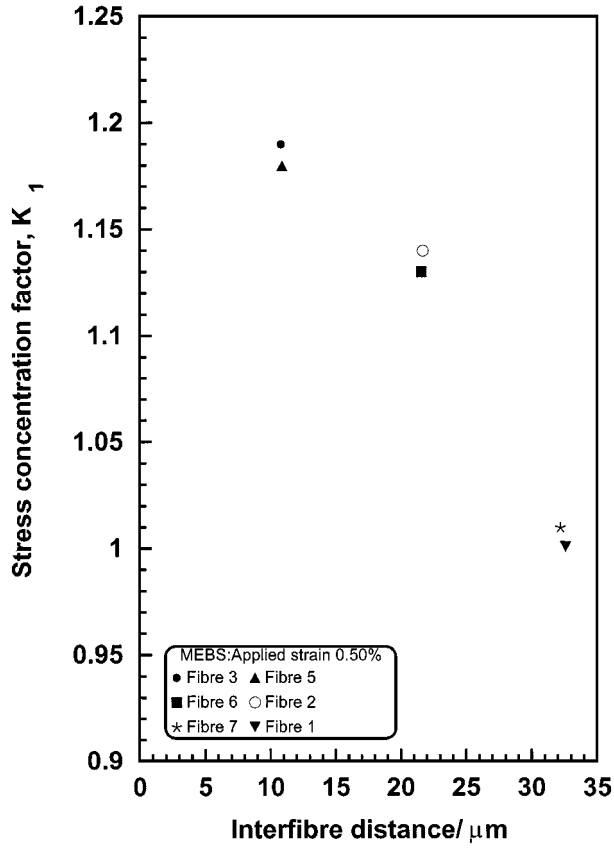

(a)

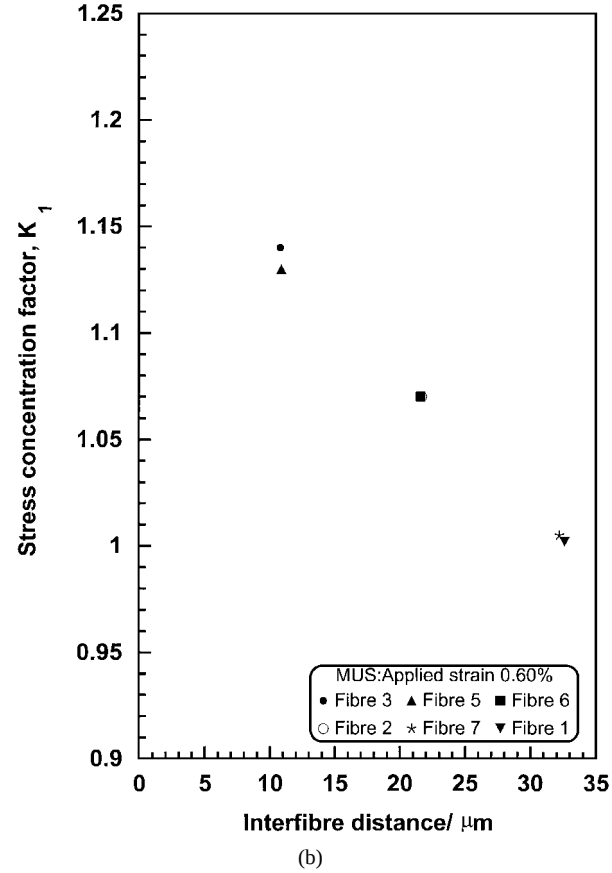

(b)

Figure 5 Calculated stress concentration factors as a function of interfibre distance for (a) MEBS tows at an applied strain of 0.50% and (b) MUS tows at an applied strain of 0.60%.

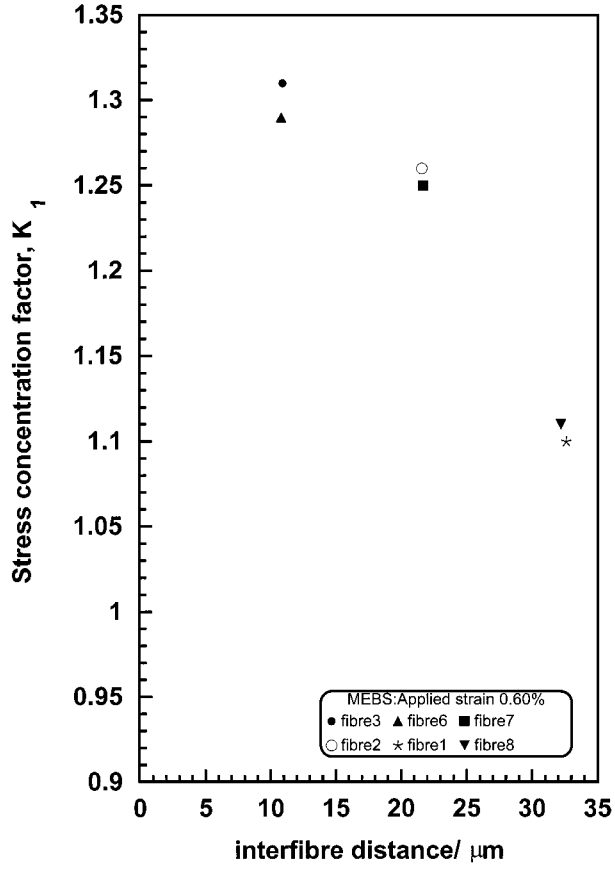

(a)

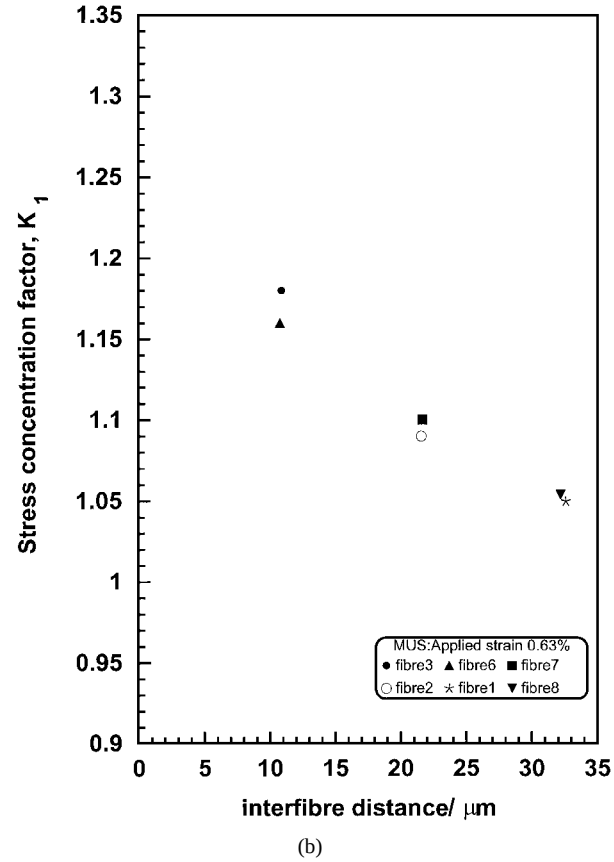

(b)

Figure 6 Calculated stress concentration factors, K_q, as a function of interfibre distance: (a) MEBS tows at an applied strain of 0.60% and (b) MUS tows at an applied strain of 0.63%.

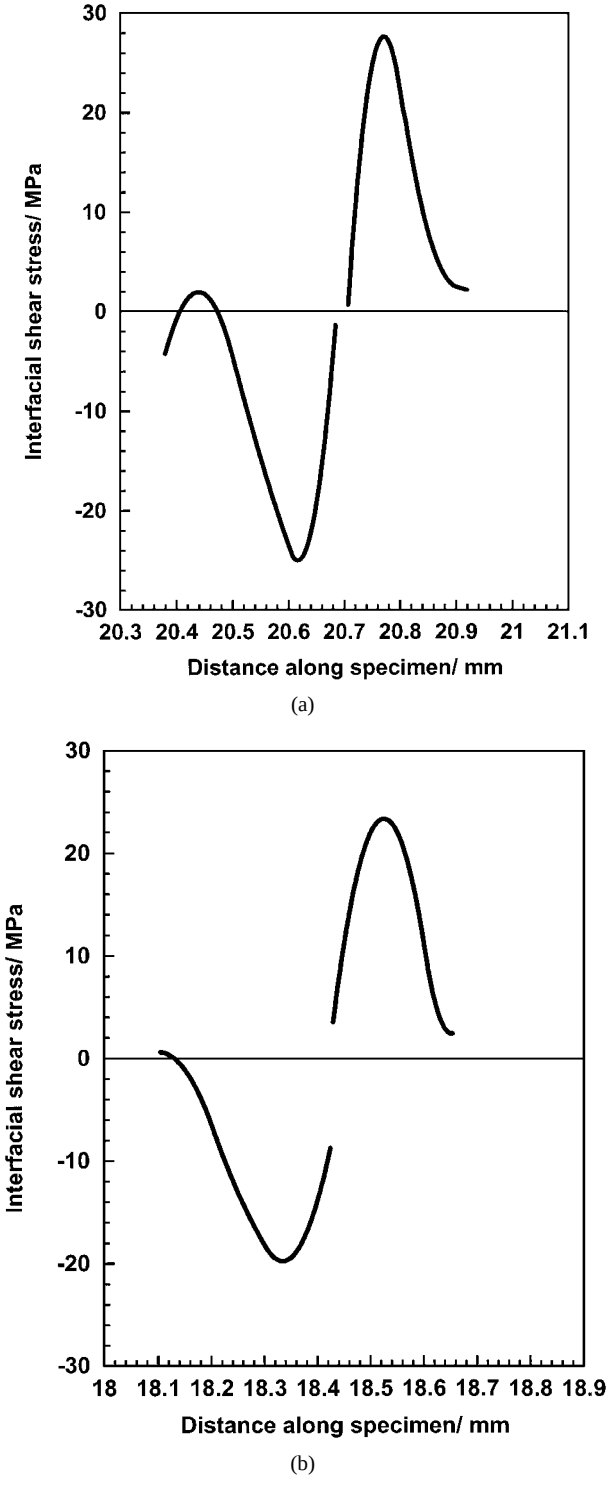

Figure 7 Interfacial shear stress distribution along fibre: (a) MEBS tows at an applied strain of 0.50% and (b) MUS tows at an applied strain of 0.60%.

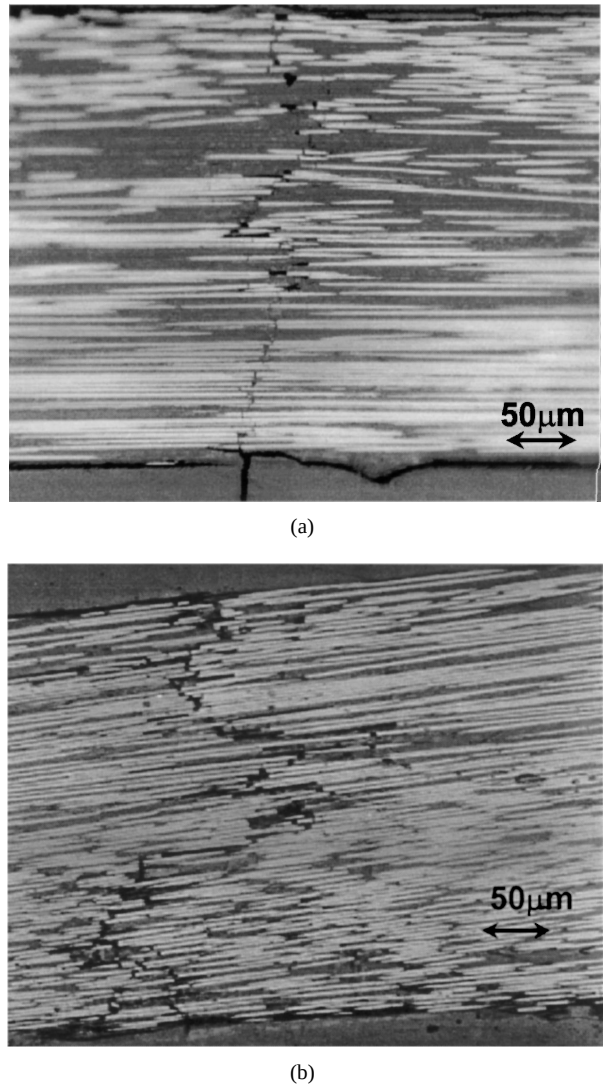

Figure 8 Photomicrographs of the failure zone of impregnated hybrid bundles (a) MEBS tows and (b) MUS tows.

unsized sample (MUS fibres) involved more debonding and fibre pullout on either side of the fracture path. This debonded region extended for approximately 1.5 mm from the crack path (Fig. 8a). In the case of the sized hybrid composite (MEBS fibres) little debonding was seen and the path of the crack traversed the tow along an axis normal to the fibres (Fig. 8b).

In Figs 9–11 the results for the MEBS and MUS tows at 0.25%, 0.35% and 0.45% applied composite strain are presented. For the sake of clarity, the neighbouring fibres in Figs 9–11 are shown equi-distant with a mean centre-to-centre interfibre distance of 10.8 ± 0.2 μm. Fibre clusters greater than a singlet have been labelled alphabetically. A summary of these data is presented in Table II.

For an applied strain of 0.25% applied strain (Fig. 9), singlets and clusters of two fibre breaks were observed in the MEBS system, whereas, only singlets were present in the case of the MUS specimens. For an applied strain of 0.35% groups of clusters greater than three were observed for the MEBS tows, whereas for the MUS samples a higher proportion of single breaks and 2-plets were seen to exist (Fig. 10). Finally, for an applied strain of 0.45% (Fig. 11), a group of 6 filament breaks (i-plets) with low overall spatial distribution is observed in the MEBS system (e.g. cluster E). In contrast, the damage in the case of the MUS sample is more widespread and the clusters are of a smaller magnitude.

Fig. 12a shows a photomicrograph of the clustering of fibre breaks in a sectioned MEBS tow at 0.45% applied strain. A 3-plet is observed at point A corresponding to Cluster B (fibres 13, 14 and 15) in Fig. 11a. Fig. 12b shows the formation of single breaks in a sectioned MUS tow at 0.45% applied strain. A singlet is

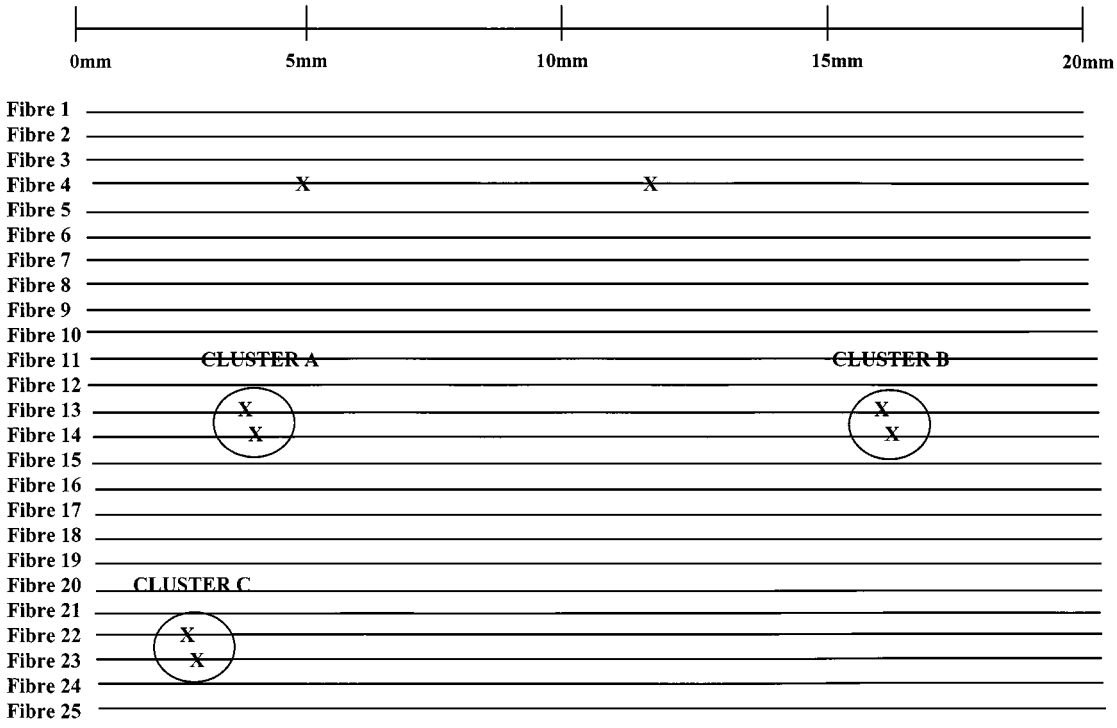

(a)

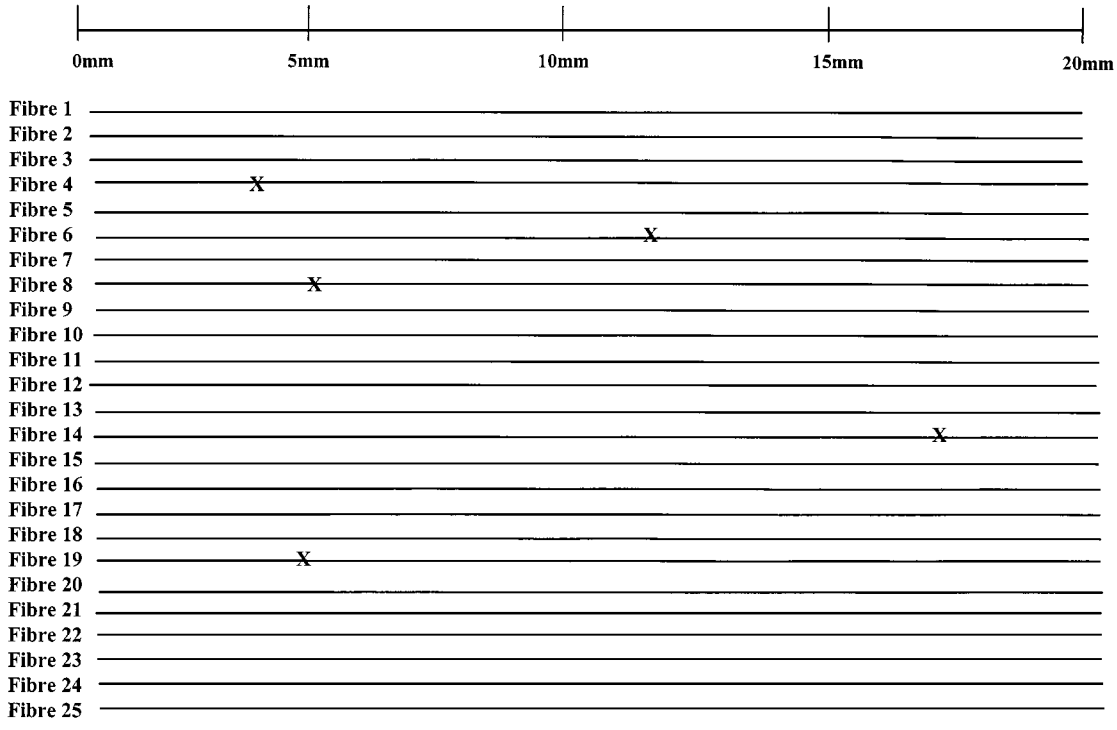

(b)

Figure 9 Fibre break investigations at 0.25% applied composite stress (a) MEBS tows and (b) MUS tows.

shown at point B (fibre 15) in Fig. 11b. The number of filament breaks at each level of applied strain is shown in Fig. 13 for both the MEBS and MUS composite systems. As expected the number of fibre fractures was found to increase with fibre strain.

The clustered MUS breaks are spread over a wide region within the 'window' of observation, as the individual failures are offset by a greater distance in comparison to the more confined MEBS damage sites (Table II). In the case of the unsized tow at 0.35% applied strain (Fig. 10b) multiple fibre breaks were detected in fibres 11 and 12 (cluster B) at a distance of 10.01 mm and 9.90 mm, which indicates that these breaks are offset by a distance 110 μm from one another. If one considers a sized cluster at 0.35% applied strain, e.g. cluster C, Fig. 10a, fibre breaks are detected in fibre 16 at 13.65 mm and fibre 17 at 13.65 mm, respectively, which indicates a much closer offset of only 20 μm.

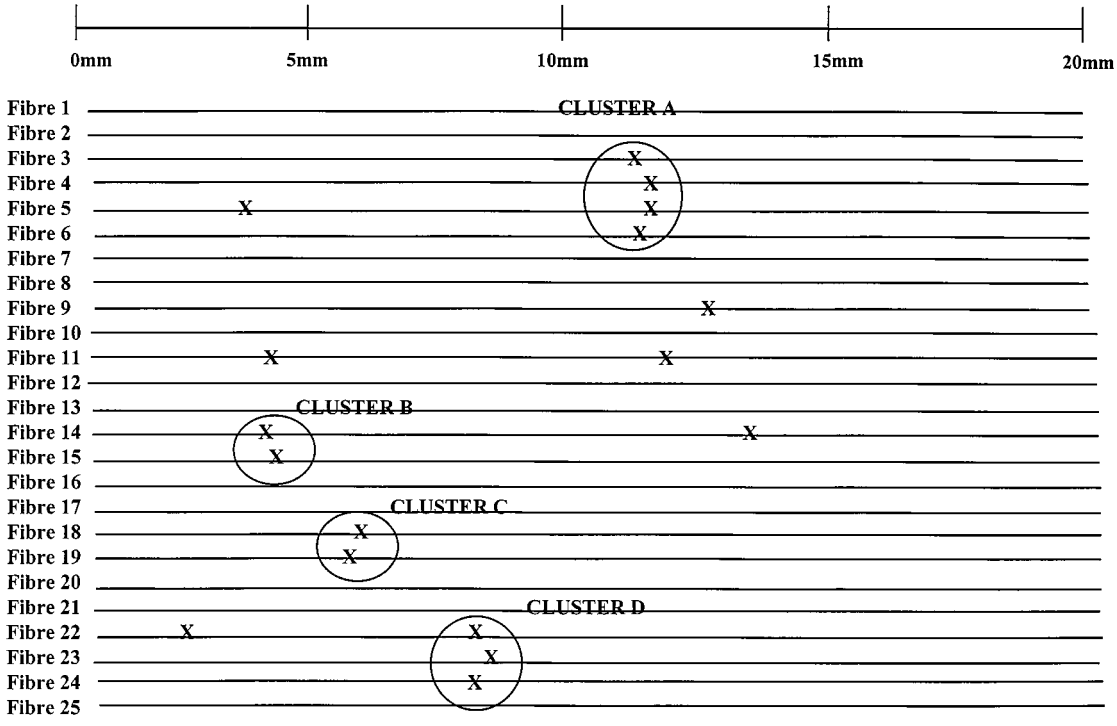

(a)

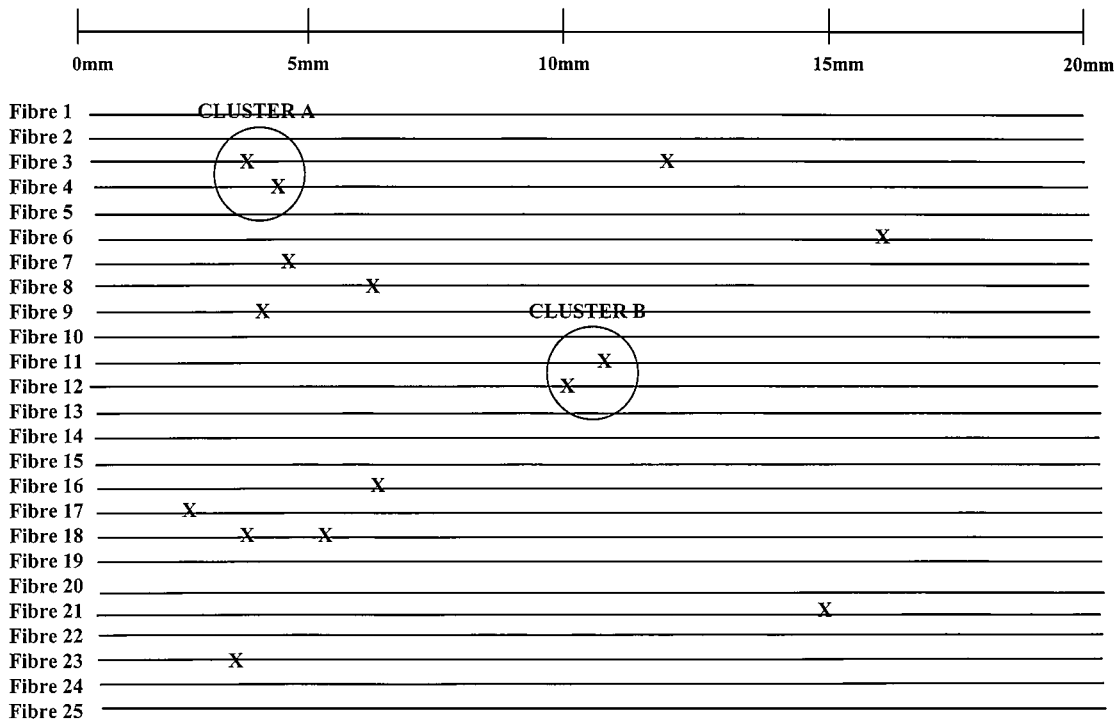

(b)

Figure 10 Fibre break investigations at 0.35% applied composite stress (a) MEBS tows (b) MUS tows.

4. Discussion

4.1. Cluster nucleation and evolution

Clusters of fibre breaks are a consequence of an aggregation of inherent filament defects. The number of these defects depends on both the level of applied stress and the magnitude of the stress concentration. If there is no fibre-fibre interaction then the strength of a fibre bundle (under Global Load Sharing conditions) is determined by the statistical accumulation of defects as mentioned in [1]. The Global Load Sharing (GLS) rule refers to an equal distribution of load from the failed fibre to the remaining intact fibres. In a composite situation the application of the GLS rule requires that these clusters are inconsequential for composite failure. However, when stress concentrations is introduced the break progression will be affected; additional breaks will be generated as a result of the stress concentration in fibres adjacent to those that have been broken initially.

In a composite there will be the generation of two types of clusters of fibre breaks; (a) 'incidental' clusters

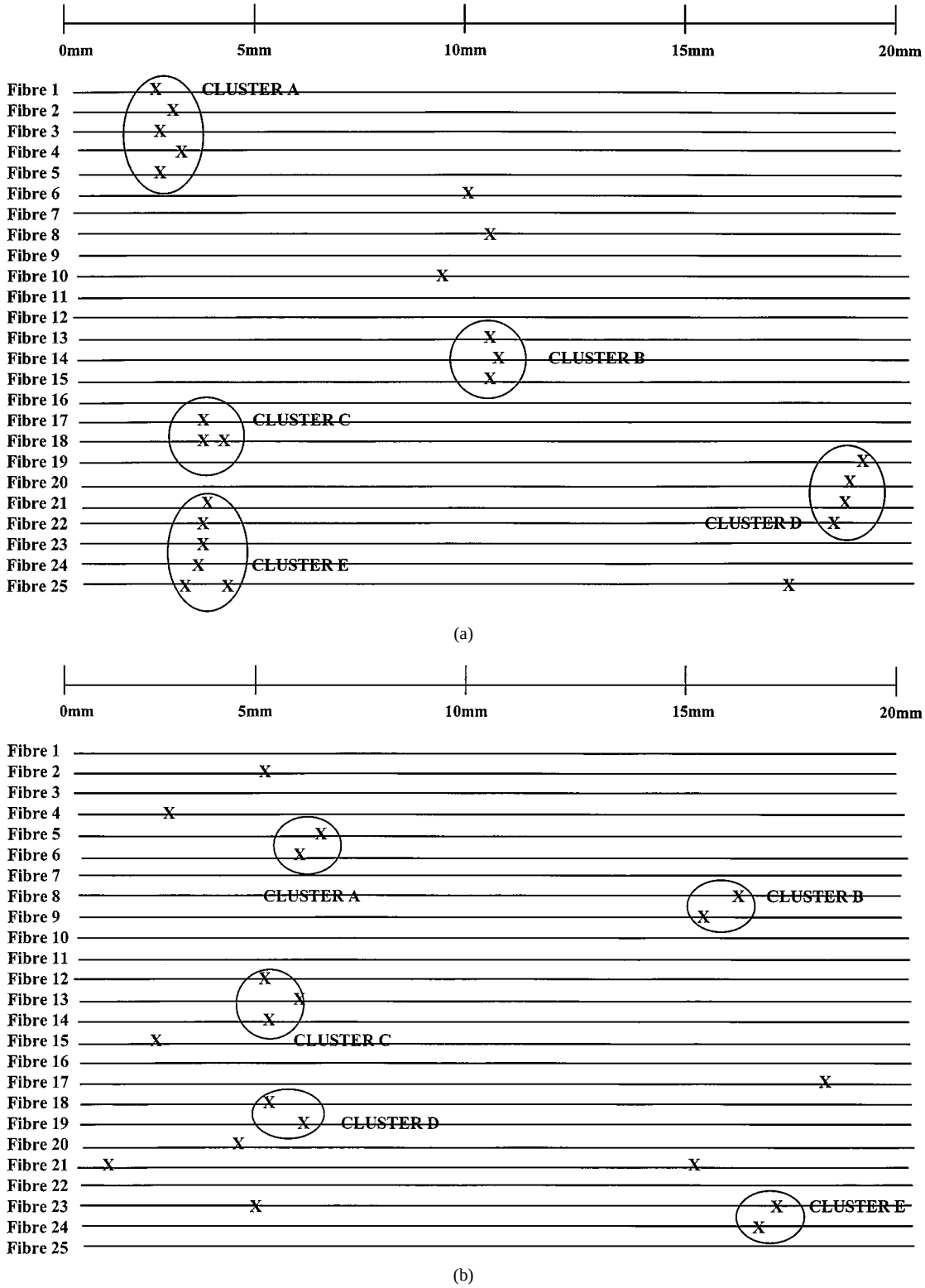

Figure 11 Fibre break investigations at 0.45% applied composite stress (a) MEBS tows and (b) MUS tows.

that will occur by pure chance due to the proximity of fibre flaws (b) 'propagating' clusters which are due to the over-stress from failed filaments. However, all breaks are still caused by the same population of defects and it is the level of applied composite stress that determines the order of cluster generation.

At fibre failure the matrix has the effect of localising the redistribution of stress to the neighbouring fibres. The rate of stress transfer is determined by the ratio of the fibre tensile modulus, E_f to the shear modulus of the matrix, G_m [21, 22]. The higher the ratio, E_f/G_m the longer the ineffective length, δ, and the lower the maximum shear stress at the fibre end. If the matrix around the fibre and the interphase region is stiff, then the stress transfers back into the broken fibres very quickly and the ineffective length is small in size. Thus the local stress concentration surrounding the filament break is higher because of the rapid nature of stress transfer in that region. Conversely, if the material surrounding the filament break is compliant, the ineffective length is large, since a large distance is required to transfer the stress back into the broken fibre.

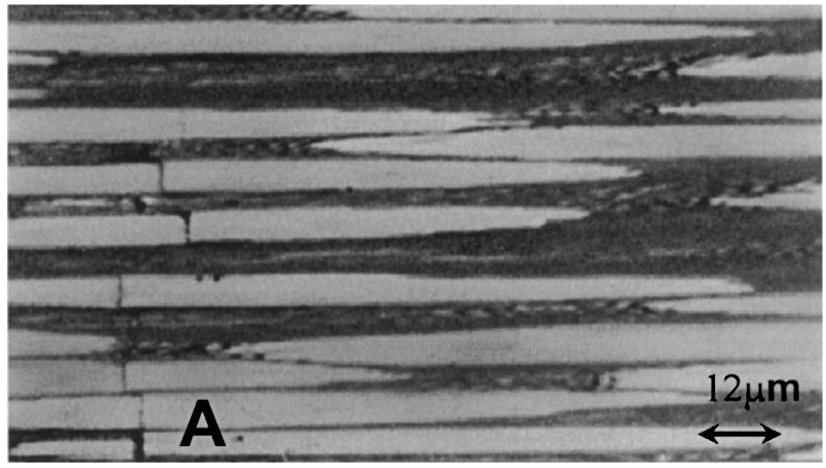

(a)

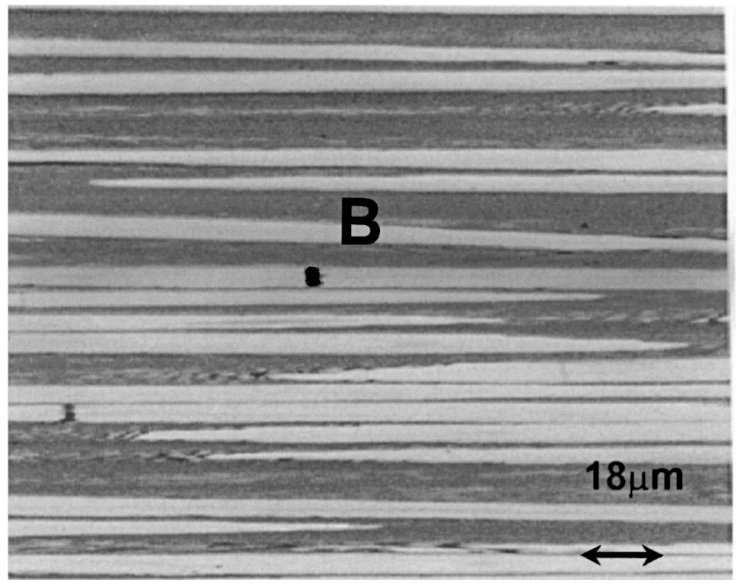

(b)

Figure 12 Photomicrographs of sectioned specimens: (a) MEBS tow at 0.45% applied strain and (b) MUS tow at 0.45% applied strain.

For the material system investigated here it is seen that at low applied stress there exists a high density of small clusters, but as the stress increases, larger clusters of lower density form. As shown in Figs 9–11, the largest *i*-plet observed for the MUS composite tows was a 3-plet, whereas for the MEBS sample, a 6-plet was observed. For the sectioned MEBS and MUS tows at 0.45% applied strain (Fig. 11a and b), the damage in the MUS tow is much more widespread but the relevant fracture sites are smaller in magnitude. The difference in cluster density between the MUS and MEBS composite systems can be explained by the higher interface strength associated with the sized tows. In the unsized fibres the bond strength is lower resulting in lower stress intensification distributed over a longer Positive Affected Length (440 μm for the MUS tow, 400 μm for the MEBS tow). In the case of the sized fibre system there is a greater probability of the increased stress in neighbouring fibres to coincide with a flaw leading to additional failures in adjacent fibres or to propagating clusters. As a result, the total number of filament failures for the sized sample per level of applied strain is greater than that of the unsized system (Fig. 13).

In Table II it is seen that the MEBS fibre breaks are more geometrically confined when compared to those of MUS filaments indicating a shorter region of influence in the neighbouring fibres. On average, the axial offset (Fig. 14) between two filament breaks in the sized (MEBS) system is approximately 37 μm. However, this value varies from cluster to cluster, with a maximum offset equal to 80 μm and the minimum corresponding to no offset between the breaks (0 μm). The average offset between breaks for the unsized system is 125 μm, with maximum and minimum value of 200 μm and 90 μm, respectively. This is expected as in the MEBS fibres greater stress intensification over a shorter PAL is obtained and this increases the probability of coinciding with a flaw in the adjacent fibres. In the MUS system, the smaller stress concentration over a longer PAL results in a smaller stress increase in the adjacent fibres, which reduces somewhat the probability of failure and cluster formation. As postulated by Sastry and Phoenix [22], a significant axial offset in 'staggered' fibre breaks of the order of 10 fibre diameters can lead to 'shielding' and, henceforth, reduction of stress concentration in adjacent fibres. Such 'staggered' fibre breaks

TABLE II Fibre break mapping for the MEBS and MUS impregnated tows at different levels of applied composite strain

	Cluster size	Cluster identifier	Fracture site		Axial off-set		No. of observations
			Fibre No.	Position (mm)	Fibre No.	Distance (μm)	
				(a) 0.25% applied strain			
Sized	1-plet		3	4.90			2
			4	12.50			
	2-plet	Cluster A	13	4.10	13/14	70	3
			14	4.17			
		Cluster B	15	15.40	15/14	50	
			14	15.35			
		Cluster C	22	3.12	22/23	20	
			23	3.10			
					Total breaks		**8**
Unsized	1-plet		4	4.43		5	
			6	11.60			
			8	5.12			
			14	17.50			
			19	4.10			
					Total breaks		**5**
				(b) 0.35% applied strain			
Sized	1-plet		5	4.50			6
			9	11.70			
			11	4.30			
			11	11.40			
			14	12.22			
			22	2.30			
	2-plet	Cluster B	14	3.63	14/15	30	3
			15	3.66	16/17	20	
		Cluster C	16	13.65			
			17	13.67			
		Cluster D	18	5.12	18/19	50	
			19	5.17			
	3-plet	Cluster E	22	7.60	22/23	60	1
			23	7.66	23/24	70	
			24	5.59			
	4-plet	Cluster A	3	11.53	3/4	30	1
			4	11.56	4/5	0	
			5	11.56	5/6	20	
			6	11.54			
					Total breaks		**19**
Unsized	1-plet		3	13.61		11	
			6	15.01			
			7	4.98			
			8	6.3			
			9	4.98			
			16	6.35			
			17	2.00			
			18	3.13			
			18	5.60			
			21	15.00			
			23	3.14			
	2-plet	Cluster A	3	3.25	3/4	96	2
			4	3.35			
		Cluster B	11	10.01	11/12	110	
			12	9.90			
					Total breaks		**15**
				(c) 0.45% applied strain			
Sized	1-plet		6	10.01			4
			8	11.2			
			10	9.8			
			25	17.13			
	3-plet	Cluster B	13	10.17	13/14	80	1
			14	10.25	14/15	40	
			15	10.21			
	4-plet	Cluster D	19	18.08	19/20	30	1
			20	18.05	20/21	20	
			21	18.03	21/22	20	
			22	18.05			
	5-plet	Cluster A	1	2.35	1/2	50	1
			2	2.40	2/3	50	
			3	2.35	3/4	0	
			4	2.35	4/5	10	
			5	2.36			

(Table continued on next page)

TABLE II (Continued)

	6-plet	Cluster E	21	3.27	21/22	30	1
			22	3.24	22/23	10	
			23	3.25	23/24	10	
			24	3.24	24/25	70	
			25	3.17	25/26	30	
			26	3.20			
					Total breaks		**22**
Unsized	1-plet		1	5.23			8
			4	3.70			
			15	3.70			
			17	17.26			
			20	5.15			
			21	1.31			
			21	15.01			
			23	5.33			
	2-plet	Cluster A	6	5.23	6/5	100	4
			5	5.33			
		Cluster B	8	16.28	8/9	200	
			9	16.08			
		Cluster D	18	5.33	18/19	130	
			19	5.46			
		Cluster E	23	17.08	23/24	150	
			24	16.93			
	3-plet	Cluster E	12	5.21	12/13	90	1
			13	5.30	13/14	130	
			14	5.17			
					Total breaks		**19**

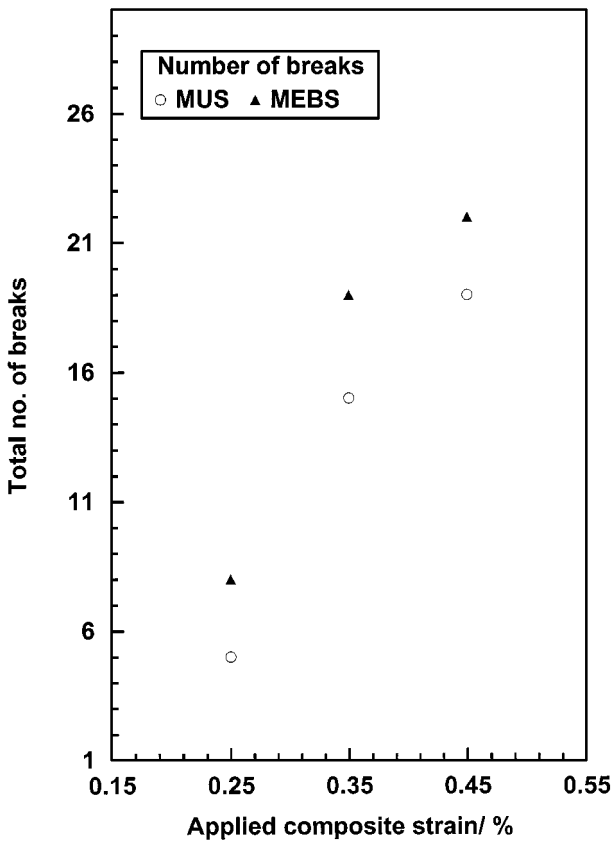

Figure 13 The cumulative number of filament breaks at each level of applied strain.

can be seen for the MEBS system in Figs 10a and 11a (clusters A, D and A, B, D and E, respectively) and for the MUS system in Fig. 11b (cluster C). The close axial proximity of the MEBS breaks (offset of less than 40 μm) makes the presence of such a 'shielding' effect questionable.

This work has shown that due to statistical nature of filament failure, clusters of fibre breaks can form in composite tows. Fibres adjacent to these clusters will be subject to a stress concentration value, K_q, which is a function of cluster density, and interface strength. By considering the cluster densities shown in Figs 9–11 it is certain that the local stress concentration will increase sharply as the number of broken fibres exceeds 6 or 7. This matches the observations that broken fibres rarely have a local group of fibre fractures that exceed 7 in carbon-epoxy material systems [24].

4.2. Mechanisms of composite failure

In a composite material the evolution of fibre break clusters and their density should be given proper attention. As in the case of the Griffith type instability [25], the number of fibre clusters increases and their size grows as the applied stress increases. At a given load, a cluster will reach a critical size and will propagate across the whole composite cross-section causing catastrophic failure. Hence, one possible mode of failure of the final composite is that due to a single nucleating site evolving into an unstable macrocrack.

In the case of the MEBS system, the ineffective length is small and the stress concentrations are high. Here there is a tendency for the neighbouring fibres to break and therefore catastrophic fracture propagates along the direction of an initial cluster. The optical micrograph of the fracture surface (Fig. 8a) shows that the failure propagates along a well-defined axis almost perpendicular to the fibre direction. This is indicative

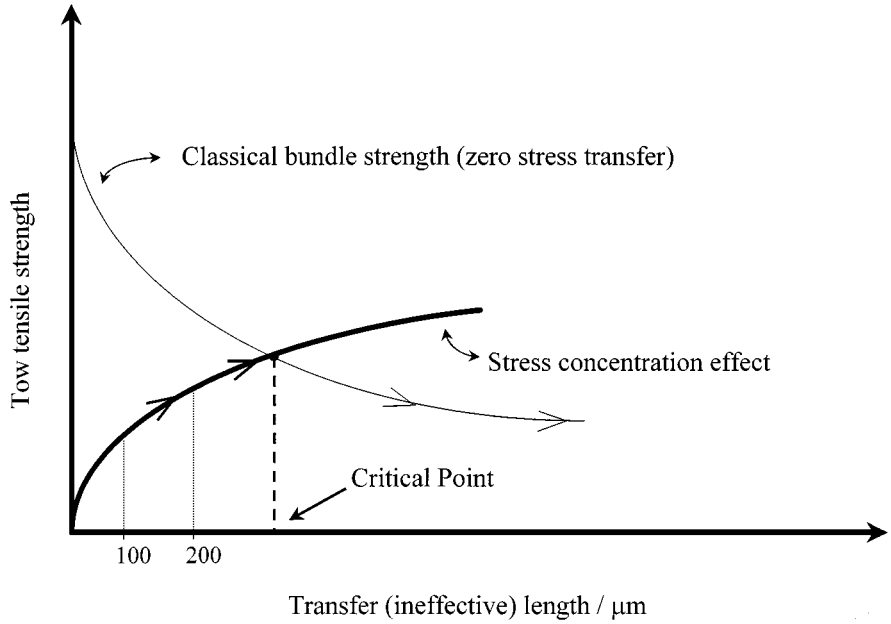

Figure 14 Schematic showing the relationship between the tow tensile strength and the ineffective length (strength of interface).

of brittle failure and is a consequence of the presence of a strong interface as mentioned earlier.

In the case of the MUS system that has inherently a weaker interface, fibre fractures are distributed over a wider region as can be seen in Fig. 11b just prior to fracture. Linking of the various clusters of low density (Fig. 11b) can occur at a high applied stress and this will ultimately lead to the failure of the whole composite cross-section. The micrograph of Fig. 8b shows that the fracture surface is considerably jagged, which is due to the fact that fracture occurs by the consolidation of clusters that are widely spaced. It is therefore conceivable that various clusters can coalesce leading to the formation of a 'supercluster' that will cause catastrophic failure of the composite. Evidently, the applied stress required to bring about fracture or in other words the static tensile strength of this type of composite should be higher than that of the sized system. Indeed, measurements of the characteristic strengths of the tow composite systems has shown that the value of the unsized system is higher by 7% (Table I) to that of the sized system. In Fig. 14a schematic of the tow tensile strength as a function of transfer length is given. For small transfer lengths, the presence of the matrix and the resulting stress concentration effect in the neighbouring fibres is more important than the reduction of strength due to fibre fracture predicted by the classical bundle strength approach [2, 16, 18]. However, the gains in the tensile strength are limited by the size of the ineffective length; there will be a critical point beyond which the reduction in the interface strength will bring about a severe reduction in the tensile strength due primarily to the loss of fibre as a means of load support (Fig. 14). The results presented here have clearly shown that the critical point in terms of ineffective length is greater or at least equal to the length of 220 μm measured for MUS tows.

Past work by Nedele and Wisnom [26] has suggested that the effect of stress concentrations in neighbouring fibres is not as significant as originally suggested by Hedgepeth [21, 27], Phoenix [22, 24, 27] and others. However, the results presented here show that the number and density of localised fibre breaks can govern the fracture process and the tensile strength of unidirectional carbon fibre/epoxy composite tows. In the second part of this series these experimental results will be examined in the light of a newly proposed statistical treatment of composite tensile strength. The model captures all the above experimental observations and can be used for quantitative strength predictions.

5. Conclusions

This work has provided an important insight into the redistribution of load around multiple filament breaks. Therefore adjacent to a fibre break there will be a critical number of more highly stressed fibres increasing the probability of fibre failure. Important parameters in the prediction of composite strength using statistical theories are the in-situ fibre statistics and the stress concentration factor in the fibres adjacent to an i-size cluster (an i-plet). Thus to improve the current models of aligned composite strength the effect of fibre surface treatment and cluster density and geometry should be taken into account in determining the values of stress concentration factors and the composite strength in general.

In a simple unidirectional composite it has been shown that the fracture relies on the interface properties that can affect the composite ultimate strength, strength variability, and failure mode/fracture morphology. In a material with a strong interface (MEBS) the fibre breaks cluster together forming an unstable microcrack. In a material with a weak interface (MUS) there is a tendency of statistical accumulation of filament failure. Final composite failure is reached where groups of widespread, low order damage can link resulting in the formation of a cluster of critical size, which propagates in an unstable fashion through the whole

composite cross section. One might, on the basis of 'bundle strength' considerations, use a stiff interface and matrix to reduce the possibility of interaction of fibre fractures at different positions along the length of neighbouring fibres. However, stress concentration effects require the reduction of the interface strength in order to reduce this stress overload. This is a problem frequently encountered in the design of the optimum tensile strength of a composite material.

Acknowledgements

One of the authors, Dr Christian Marston, gratefully acknowledges the support of South Bank University, in particular Dr Brian Gabbitas and Mr Jack Adams Bank for advice and guidance in this research programme. Many valuable discussions with Dr Jonas Neumeister of the Aeronautical Research Institute of Sweden (FFA) are acknowledged.

References

1. B. W. ROSEN, *AIAA Journal* **2** (1964) 1985–1991.
2. C. ZWEBEN and B. W. ROSEN, *J. Mech. Phys. Solids.* **18** (1970) 189–206.
3. R. L. SMITH, *Proc. Roy. Soc. London* **A372** (1980) 539–553.
4. D. G. HARLOW and S. L. PHOENIX, *J. Comp. Mater.* **12** (1978) 195–215.
5. D. G. HARLOW and S. L. PHOENIX, *ibid.* **12** (1978) 314–334.
6. M. G. BADER, *Sci. Eng. Comp. Mater.* **1** (1988) 1–11.
7. S. B. BATDORF, *J. Reinf. Plas. Comp.* **1** (1982) 152–164.
8. D. HULL, "An Introduction to Composite materials," Cambridge Solid State Series (Cambridge University Press, Cambridge 1981).
9. W. WEIBULL, *J. Appl. Mech.* **18** (1951) 293–296.
10. P. W. BARRY, *J. Mater. Sci.* **13** (1978) 2177–2187.
11. Z. GAO, K. REIFSNIDER and G. CARMAN, *J. Comp. Mater.* **26/11** (1992) 1678–1705.
12. J. NEUMEISTER, personal communication.
13. A. PAIPETIS and C. GALIOTIS, *Composites* **27A** (1996) 755–767.
14. DRZAL ET AL., *J. Adhesion* **16** (1983) 1–30.
15. Ciba Geigy, Data sheets and technical notes on Matrix systems, Publication no. 38285/1/e, 1995.
16. C. MARSTON, Ph.D thesis, South Bank University, London, 1997.
17. ASTM D3379-75, "Tensile strength and Young's modulus for high modulus single-filament material. Book of ASTM Standards," Vol. 7 (American Society for Testing and Materials, 1989) 731–785.
18. C. MARSTON, B. GABBITAS, J. ADAMS, S. NUTT, P. MARSHALL and C. GALIOTIS, *Composites* **27A** (1996) 1183–1194.
19. C. MARSTON, B. GABBITAS and J. ADAMS, *J. Mater. Sci.* **32** (1997) 1415–1423.
20. C. MARSTON, B. GABBITAS, J. ADAMS, P. MARSHALL and C. GALIOTIS, *Comp. Sci. Technol.* **57** (1997) 913–923.
21. J. M. HEDGEPTH, Stress concentrations in filamentary structures, Technical note, D-882, NASA, Washington, 1961.
22. A. M. SASTRY and S. L. PHOENIX, *Soc. Adv. Mater. Process Eng. J.* **30** (1994) 61–67.
23. C. GALIOTIS, *Comp. Sci. Technol.* **48** (1993) 15–28.
24. D. G. HARLOW and S. L. PHOENIX, *Intl. J. Fracture* **17** (1981) 321–336.
25. A. A. GRIFFITH, in Proceedings of the First International Congress for Applied Mechanics, Delft (1924) pp. 55–63.
26. M. WISNOM and D. GREEN, *Composites* **26** (1995) 499–508.
27. I. BEYERLEIN and S. L. PHOENIX, *Comp. Sci. Technol.* **57** (1997) 869–885.

Received 12 August
and accepted 14 September 1998